Available online at www.sciencedirect.com
ScienceDirect
Biochemical and Biophysical Research Communications 353 (2007) 115–120
BBRC
www.elsevier.com/locate/ybbrc

Structural analysis of the 26S proteasome by cryoelectron tomography

Stephan Nickell, Oana Mihalache, Florian Beck, Reiner Hegerl, Andreas Korinek, Wolfgang Baumeister *

Max-Planck-Institute of Biochemistry, Department of Structural Biology, Am Klopferspitz 18, D-82152 Martinsried, Germany

Received 20 November 2006
Available online 6 December 2006

Abstract

The 26S proteasome is the key enzyme of intracellular protein degradation in eukaryotic cells. It is a multisubunit complex of 2.5 MDa confining the proteolytic action to an inner compartment with tightly controlled access. Structural studies of this intriguing molecular machine have been hampered by its intrinsic instability and its dynamics. Here we have used an unconventional approach to obtain a three-dimensional structure of the holocomplex uncompromised by preparation-induced alterations and unbiased by any starting model. We have performed a tomographic reconstruction, followed by averaging over approx. 150 individual reconstructions, of *Drosophila* 26S proteasomes suspended in a thin layer of amorphous ice.

Keywords: 26s; Proteasome; Electron tomography

Protein degradation is a key regulatory element controlling a large variety of cellular functions. Eukaryotic cells possess two major proteolytic systems, the lysosomal proteases and the 26S proteasome, a multi-subunit complex of approx. 2.5 MDa [1]. The 26S proteasome acts at the downstream end of the ubiquitin pathway; ubiquitin is covalently attached to proteins destined for degradation. Proteins tagged with multiubiquitin chains are selected by the 26S complex and degraded in an ATP-dependent process [2–5]. Whereas the lysosome is a membrane-bound cellular compartment containing several small proteases, the 26S proteasome is a self-compartmentalizing protein assembly comprising more than 30 different subunits [6]. Two major subcomplexes jointly form the 26S (more accurately the 30.3S, [7]): the barrel-shaped proteolytic core complex (the 20S proteasome) and the regulatory (19S) complexes, which associate with either one (single capped) or both ends (double capped) of the core complex [8]. While the structure and function of the 20S proteasome have been studied in great detail [9,5], our understanding of the structure and mode of operation of the holocomplex is still substantially incomplete. The main role of the regulatory complexes is to prepare substrates for degradation in the 20S core complex. This involves the recognition and binding of ubiquitylated substrates, their deubiquitylation, the unfolding of substrates which is necessary for admission to the 20S core, and assistance in their translocation [10,11].

Structural studies of 26S proteasomes are hampered by the low intrinsic stability of the holocomplex, which easily dissociates into subcomplexes and by its dynamics [12]. As a consequence, electron micrographs of 26S preparations display a degree of structural heterogeneity that complicates image analysis and three-dimensional (3D) reconstruction. Hitherto all electron microscopy studies of the 26S complex were based on negatively stained preparations. Images of negatively stained samples have the advantage of a relatively high signal-to-noise ratio, but at the expense of additional risks of structural alterations. These in turn could be caused by the adsorption of this rather labile structure to the supporting carbon film or by the heavy metal salts used for staining. Therefore, in order to

* Corresponding author. Fax: +49 89 8578 2641.
E-mail address: baumeist@biochem.mpg.de (W. Baumeister).

0006-291X/$ - see front matter © 2006 Elsevier Inc. All rights reserved.
doi:10.1016/j.bbrc.2006.11.141

obtain a faithful structure, it is clearly desirable to perform a three-dimensional structural analysis of the 26S proteasome suspended in a thin layer of vitreous ice. Single particle 3D reconstructions based on angular reconstitution, as commonly practiced nowadays [13], rely on the assumption that the particles are randomly oriented in the ice layer, which is not necessarily the case, in particular when structures are rather elongated, as the 26S complex is. To avoid this problem, we have chosen a tomographic reconstruction scheme followed by the averaging of the individually reconstructed particles. This approach, which is similar to the one applied previously to thermosomes [14] and tricorn protease [15], has the advantage that no assumptions (such as similarity to a reference or symmetry) have to be made in the reconstruction process. Since the 3D averaging was also done in a manner minimizing any bias, using an almost featureless reference, the resulting structure can be regarded as highly trustworthy.

Materials and methods

Isolation and purification of 26S proteasomes from Drosophila. 26S proteasomes were purified as described in detail previously [16,12]. Briefly, 0–16-h *Drosophila* embryos (Yellow white strain) were collected at 25 °C from feeding plates. After dechorionation and homogenization, the extract was clarified by centrifugation and nucleic acids were removed by precipitation with 10% streptomycin sulfate. The supernatant was fractionated with hydroxyapatite in a batch procedure, followed by anion-exchange chromatography (diethylaminoethyl cellulose, DE52, Whatman) and sucrose density gradient centrifugation (15–40% sucrose). At all stages, fractions were tested for their ability to hydrolyze succinyl-Leu-Leu-Val-Tyr-7-amido-4-methylcoumarin (Suc-LLVY-AMC; Bachem), and only fractions containing the peaks of activity were used for further purification. Active fractions were examined by electron microscopy and only fractions with large numbers of intact double-capped complexes were used for cryoelectron microscopy.

Electron microscopy. Four-microliter droplets of buffer solution containing 26S proteasomes were applied to lacey carbon grids previously rendered hydrophilic in a plasma cleaner. Excess suspension was removed after 60 s by blotting with filter paper. After a short washing step, using a few microliters of distilled water, the grid was blotted again and plunged into liquid ethane for vitrification. Tomographic data sets were recorded in a fully automated manner using a CM 200 FEG transmission electron microscope (FEI, Eindhoven, The Netherlands) equipped with a cryo-holder, and a slow-scan CCD camera. The experimental set-up has been described by [17] and [14]. The accelerating voltage was 160 kV, the total magnification on the CCD-plane was 36,000×, corresponding to a 0.39 nm pixel size in the object-plane. For all samples, the defocus was set to values between 2.5 and 3.0 μm underfocus; at this setting the first zero of the contrast transfer function was beyond $(2.9\ \text{nm})^{-1}$ in all images. Data were collected from thin (50–80 nm) self-sustaining ice regions spanning the holes in the carbon film, close to an edge of the carbon film in order to reduce charging effects. The range of tilt angles used was −60° to +60°, with 5° angular increments. The cumulative dose used for recording the tilt series was kept at a subcritical level—approximately at ∼2000 electrons nm^{-2}. In addition to the tilt-series, projection images of 26S samples were recorded with a Polara G^2 (FEI, Eindhoven, The Netherlands) microscope equipped with a GIF 2002 energy filter using automated procedures implemented in the TOM software toolbox [18].

Image processing. Image processing was carried out on Linux workstations using Matlab (The Mathworks, Natick, USA) and the TOM toolbox [18]. Reconstruction and alignment of the 26S proteasome particles were performed as follows: for tomographic reconstructions, 12 tilt series were selected and aligned using gold beads as fiducial markers which had been added to the sample prior to cryo-fixation. Three-dimensional reconstructions were calculated by means of a weighted backprojection algorithm. In order to localize individual 26S proteasomes in the tomograms, overview reconstructions ($512 \times 512 \times 128$ voxels) were obtained and the positions of the particles were determined visually in an interactive manner.

All together, 412 individual pre-selected particles were reconstructed in subvolumes with a size of $128 \times 128 \times 128$ voxels at the full resolution (pixel size of 0.39 nm). In an initial alignment step, all particles were oriented with respect to a cylindrical template (with the long axis in the x–y plane) by an exhaustive six-dimensional angular and translational search based on normalized cross-correlation [19]. In a second selection step, the aligned particles were displayed and all double-capped 26S complexes were selected interactively. A total of 153 particles were processed further. Using again a cylinder-shaped template as a start reference, the particles were iteratively aligned on the basis of the locally normalized cross-correlation, including a correction for the varying orientation of the missing wedge. During this iteration, the angular scanning increment was stepwise reduced from 30° to 4°. After each iteration cycle, an average was calculated, applying an exact weighting function hereby correcting for different overlapping regions of particles in Fourier-space. This average was then used as a reference for the following cycle. The iteration was stopped when changes between subsequent averages became insignificant. The whole procedure was repeated using the last obtained average as a start reference and with angular increments starting from 10° down to 2°. Additional refinement runs did not yield significant improvements in the alignment parameters.

Finally, the tomographic average was centered and oriented along the pseudo-sevenfold axis of the 20S core particle. The average was cut in the middle such that both halves comprised half of a 20S core particle and one 19S regulatory complex. The alignment parameters of both halves were determined by applying an exhaustive six-dimensional search algorithm. As expected, it was found that the 26S proteasome complex has a C_2-symmetry axis perpendicular to the pseudo-sevenfold axis of the 20S particle and therefore this symmetry was applied to the average.

The resolution of the 3D structures was estimated using Fourier shell correlation [20]. All shown tomographic densities were low-pass filtered to a resolution of 3.5 nm. Isosurface representations were generated with the Amira software (Mercury computer Systems Inc., Chelmsford, USA). The threshold was set to include a protein mass of 2.5 MDa [6] assuming a mass density of 1.3 g/cm^3. From the projection images class-averages were calculated using a projection-refinement procedure [21] implemented in the TOM toolbox.

Results

Drosophila melanogaster embryos are a good source for obtaining 26S proteasomes which are well defined in subunit composition and suitable for structural studies [12,6]. But in spite of all efforts to maintain the integrity of the holocomplex throughout purification and sample preparation for electron microscopy, the preparations are heterogeneous: 26S complexes, single- and double-capped, coexist with 20S core and 19S regulatory complexes (Fig. 1a). 20S particles, most of them seen end-on in self-sustaining regions of the ice layer are the dominant species (65% of the total population) owing to their relatively high stability. Double-capped 26S complexes in a side-on orientation represent only a minor class (∼15%) but are nevertheless abundant enough for an in-depth structural analysis. It is not always possible to judge, based upon inspection of the projection images, to what class a given particle belongs; often only the tomographic reconstruction gives an unambiguous answer. For example, many of the

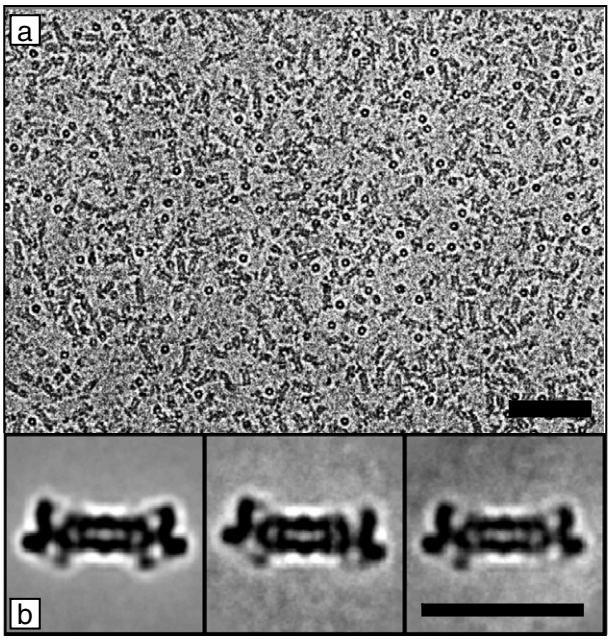

Fig. 1. (a) Overview electron micrograph of ice-embedded proteasome complexes. Isolated core particles namely 20S proteasomes and single-capped 26S complexes are mostly visible as 'top' views (circular shapes) while double-capped 26S proteasomes appear as 'side' views. In this study only 26S complexes with two 19S cap complexes were analyzed. The scale bar corresponds to 150 nm. (b) Class averages of typical side views of 26S complexes. The scale bar corresponds to 45 nm.

ring-like structures seen in Fig. 1a represent single-capped 26S complexes oriented with the long (pseudo-sevenfold) axis nearly perpendicular to the plane of the ice layer. We have based all further analyses entirely on clearly recognizable double-capped holocomplexes. Classification and averaging of two-dimensional projections of the complexes (Fig. 1b) show the typical appearance of the complex as familiar from negatively stained samples. As can be expected, the 19S caps are variable in their appearance because the asymmetric regulatory complexes vary in orientation (mainly a rotation around the long axis) while the pseudo-sevenfold symmetry core complex appears invariable at low resolution.

In three-dimensional reconstructions of individual 26S holocomplexes the main features are clearly recognizable—in spite of the poor signal-to-noise ratio of the tomograms (Fig. 2a). After alignment and averaging of 153 particles (selected out of an initial data set of 412) (Fig. 2b) the structure is rather well defined and adding more particles does not substantially improve the data quality because resolution is currently limited by electron optical settings.

The orientation of the particles in the 50–80 nm thick ice films is distinctly nonrandom, which is not surprising given that the length of the holocomplex (45 nm) is in the same size range. As shown in Fig. 3a, a large fraction of the particles is oriented in such a way that this long axis is inclined by approx. 30° with respect to the plane of the ice layer. But because of the combined effects of tilting the sample $\pm 60°$ and variations in their orientation, the cone-shaped region in Fourier space that remained unsampled is rather small and as a consequence resolution is nearly isotropic (Fig. 3b). According the Fourier-shell correlation and using the conservative 0.5 correlation coefficient criterion, resolution of the averaged tomograms is 4.6 nm (Fig. 3c). This is on one hand inferior to the resolution obtained previously with negatively stained preparations [12]; but on the other hand, by avoiding artefact-prone sample preparation procedures, and by performing the reconstruction in an objective and unbiased manner, the resulting structure is much more reliable.

Fig. 4 shows different views of the averaged 26S proteasome, rotated around the long axis, both in isosurface representations and in the form of orthoslices of the tomographic density. For comparison, we have superimposed onto the isosurface representation (which was thresholded to accommodate a protein mass of 2.5 MDa, as experimentally determined) a space-filling representation of the 20S core structure derived from the Thermoplasma acidophilum proteasome crystal structure [22] by low-pass filtering. The agreement with this internal 'gold standard' is

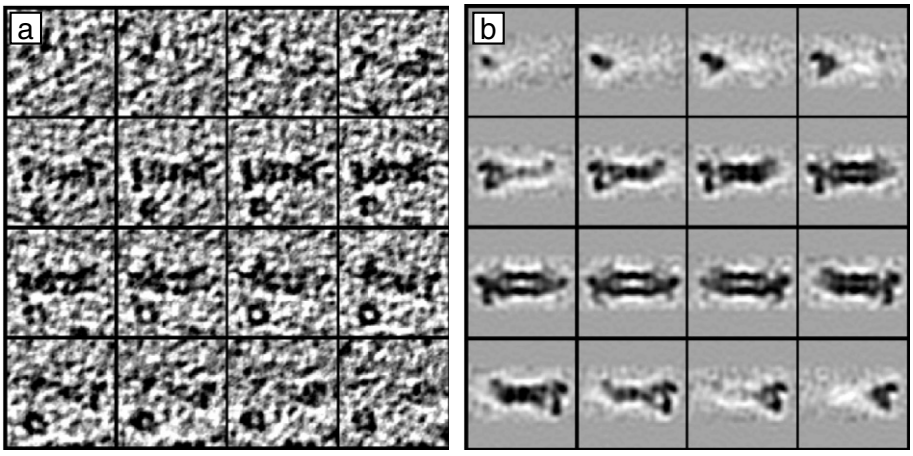

Fig. 2. (a) Gallery of x–y slices showing a single tomographic reconstruction of a 26S proteasome complex. (b) Gallery of x–y slices of the tomographic average totalling 153 individual tomograms after six-dimensional alignment and C_2-symmetrization.

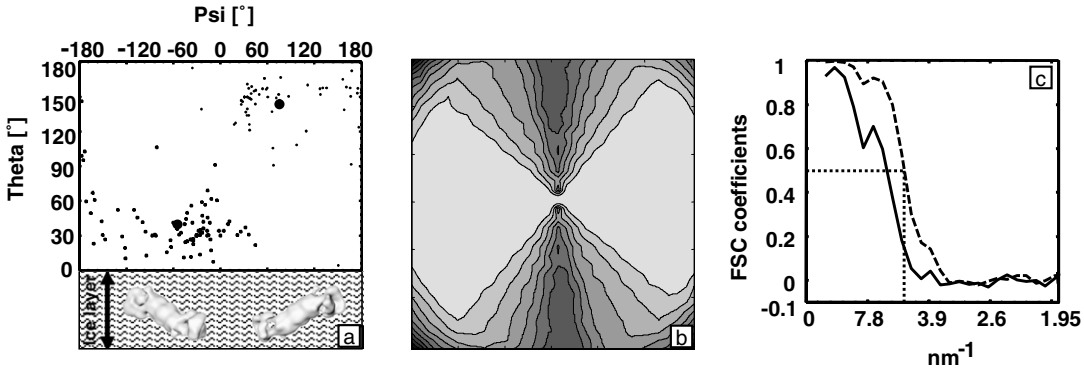

Fig. 3. (a) Angular distribution of ice-embedded particles. Most 26S complexes show a preferred horizontal orientation in the ice layer. The angle *Theta* describes a rotation around the sevenfold axis of the 20S core complex, the angle *Psi* describes a rotation around the twofold axis of the 20S core. By applying cluster analysis two centroids of the angular distribution were determined (indicated as solid dots). The bottom part of the figure shows two isosurface representations of the 26S proteasome complexes rotated according to the two centroids of the angular distribution. The textured area represents an ice-layer with a typical thickness of approximately 50 nm. (b) Central slice through the three-dimensional weighting function in Fourier-space illustrating the angular coverage of the data. Most particles were oriented as 'side' views which is reflected in Fourier-space by a stronger horizontal signal. Less signal is present along the vertical direction. Due to the random distribution of in-plane rotations of the averaged particles the weighting function is almost symmetric around the vertical axis. Consequently only a small 'missing cone'-shaped region is not sampled at all. (c) Fourier-shell correlation function calculated from two separate sets of particles. The dashed line shows the resolution after applying a C_2 symmetry to the set of data. The dotted line at a Fourier-shell correlation coefficient of 0.5 indicates a resolution of 4.6 nm^{-1}.

remarkably good, indicating that the whole structure is also highly trustworthy.

The average structure of the 26S proteasome, while corroborating known basic features, such as the mode of association of the two 19S regulatory complexes with the core complex, also shows features which are new or at variance with the negative stain structure. We see, for example, for the first time, a dome-shaped cavity under the base part of the regulatory complex, i.e., proximal to the core, which is similar in size to the central chamber and the two antechambers of the core complex. Although resolution is not good enough to outline and assign subunits of regulatory complex to its 3D structure, this suggests that the AAA-ATPases, which are located in the base part of the eukaryotic holocomplex [11] are organized in a similar manner as their much simpler archaeal counterparts [23] or the bacterial Clp and HsLV/HsLU complexes [24,25]. The new data also indicate (see top row in Fig. 4) that there is a sideward channel connecting the cavity underneath the base with the outside. It could provide an entry or exit site for substrate. A substantially improved resolution will be required to describe the structural properties of this channel and its precise dimensions or to assign the 18 constitutive subunits of the 19S cap to structural features.

Discussion

The 26S proteasome play a key role on a plethora of cellular processes [5]. It's mechanism of action however, is only poorly understood and there is no solid structural framework to explain many of its functions. The sheer complexity of this 2.5 MDa complex together with its low intrinsic stability have hitherto made a detailed structural analysis impossible. Here we have chosen an unconventional strategy to obtain a structure which can be regarded as trustworthy. By examining the holocomplex embedded in vitreous ice we avoided the risk of artifacts arising from negative staining, in particular with labile structures. And by using a tomographic approach for reconstruction, we eliminated any bias, due to avoiding the choice of an initial reference or starting model.

Alignment is usually based on calculating the cross-correlation function (CCF) between repetitive structures. The higher the number of information elements (pixels, voxels) and the more characteristic features these elements collectively form, the better defined the resulting CCF is. As a consequence, since a 3D map of an object contains more information than a single projection image of the same object, the alignment of tomographic data, is superior in terms of reliability to the alignment of projection data.

The resulting model, albeit modest in terms of resolution, is not only much more reliable than previous models, it also shows some new and interesting features, such a dome-shaped cavity underneath the base of the regulatory complex, or a channel connecting this cavity with the outside. The present model provides a solid platform now for refinements aiming at a much improved resolution. Although there is scope for improvement (dual-axis tilting, higher magnification), continuing with a purely tomographic approach may not be the most efficient way to attain higher resolution. Now that a robust starting model is at hand and can be used as an initial reference, it might be advantageous to use a hybrid approach combining tomography with single particle analysis. This experimental strategy has to take into account the fact that the vast majority of particles occur in a side-view orientation with only relatively small deviations from a plane parallel to the ice layer resulting in incomplete sampling (missing

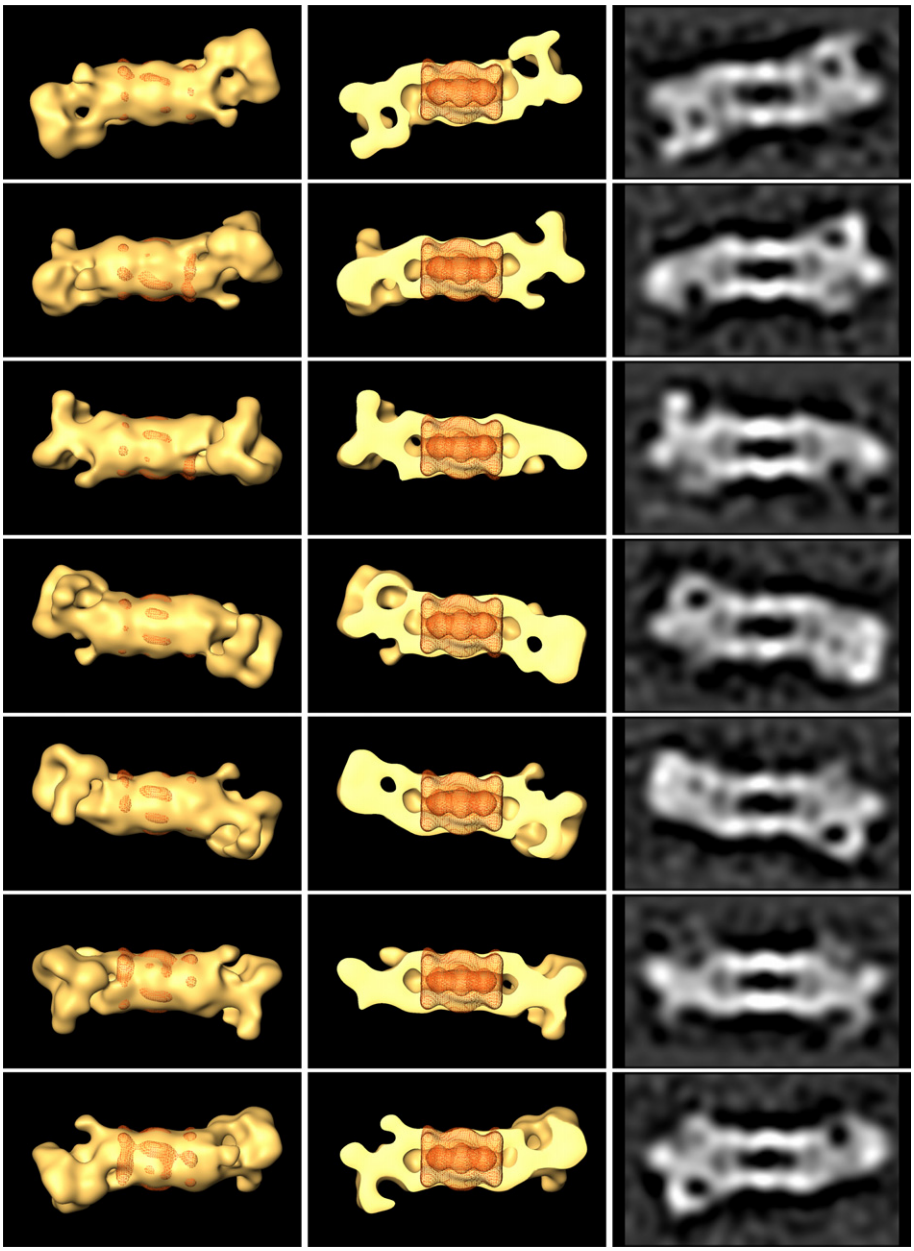

Fig. 4. The left and center column show isosurface representations of the tomographic average of the 26S proteasome complex. The view direction corresponds to the C_2-axis of the 20S core particle. The isosurface threshold was set to include a protein mass of 2.5 MDa. The crystal structure of the 20S catalytic core particle of *Thermoplasma acidophilum* was low-pass filtered to a resolution of 3.5 nm (red mesh) and fitted by an extensive-search correlation algorithm. From top to bottom a rotation around the sevenfold axis of the 20S particle was applied resulting in seven different views of the complex. The center column shows isosurfaces of the half-cut tomographic average while in the right column central orthoslices of the density distribution (inverted) of the tomographic average are displayed.

'cone' in Fourier space). To overcome this limitation to single particle analysis and to acquire images from an extended range, the specimen should be pretilted. As a consequence of this tilt, the sample thickness will increase and the signal-to-noise ratio will become lower. Pretilting the specimen by 30–45° will increase thickness by factors of 1.15–1.41, which would be tolerable. Similarly the focus gradient caused by the tilting has to be taken into account and to be corrected for in image processing. Finally, the relatively low proportion of intact holocomplexes requires that very large data sets must be recorded; automated single-particle data acquisition schemes will greatly facilitate this endeavor.

Acknowledgments

This work was supported by the 3-D Repertoire grant and the 3-D EM Network of Excellence grant within the Research Framework Programme 6 (FP6) of the European Commission.

References

[1] W. Baumeister, J. Walz, F. Zuehl, E. Seemueller, The proteasome: paradigm of a self-compartmentalizing protease, Cell 92 (1998) 367–380.

[2] A. Hershko, A. Ciechanover, The ubiquitin system, Annu. Rev. Biochem. 67 (1998) 425–479.

[3] O. Coux, K. Tanaka, A.L. Goldberg, Structure and functions of the 20S and 26S proteasomes, Annu. Rev. Biochem. 65 (1996) 801–847.

[4] Z.G. Zhang, A. Clawson, M. Rechsteiner, The proteasome activator 11S regulator or PA28—Contribution by both alpha and beta subunits to proteasome activation, J. Biol. Chem. 273 (1998) 30660–30668.

[5] D. Voges, P. Zwickl, W. Baumeister, The 26S proteasome: a molecular machine designed for controlled proteolysis, Annu. Rev. Biochem. 68 (1999) 1015–1068.

[6] H. Hölzl, B. Kapelari, J. Kellermann, E. Seemuller, M. Sumegi, A. Udvardy, O. Medalia, J. Sperling, S.A. Muller, A. Engel, W. Baumeister, The regulatory complex of *Drosophila melanogaster* 26S proteasomes: subunit composition and localization of a deubiquitylating enzyme, J. Cell Biol. 150 (2000) 119–129.

[7] T. Yoshimura, K. Kameyama, T. Takagi, A. Ikai, F. Tokunaga, T. Koide, N. Tanahashi, T. Tamura, Z. Cejka, W. Baumeister, K. Tanaka, A. Ichihara, Molecular characterization of the 26s proteasome complex from rat-liver, J. Struct. Biol. 111 (1993) 200–211.

[8] J.M. Peters, Z. Cejka, J.R. Harris, J.A. Kleinschmidt, W. Baumeister, Structural features of the 26-S proteasome complex, J. Mol. Biol. 234 (1993) 932–937.

[9] M. Bochtler, L. Ditzel, M. Groll, C. Hartmann, R. Huber, The proteasome, Annu. Rev. Biophys. Biomol. Struct. 28 (1999) 295.

[10] A. Lupas, A.J. Koster, W. Baumeister, Structural features of 26S and 20S proteasomes, Enzyme Protein 47 (1993) 252–273.

[11] M.H. Glickman, D.M. Rubin, O. Coux, I. Wefes, G. Pfeifer, Z. Cjeka, W. Baumeister, V.A. Fried, D. Finley, A subcomplex of the proteasome regulatory particle required for ubiquitin-conjugate degradation and related to the COP9-signalosome and eIF3, Cell 94 (1998) 615–623.

[12] J. Walz, A. Erdmann, M. Kania, D. Typke, A.J. Koster, W. Baumeister, 26S proteasome structure revealed by three-dimensional electron microscopy, J. Struct. Biol. 121 (1998) 19–29.

[13] J. Frank, Single-particle imaging of macromolecules by cryo-electron microscopy, Annu. Rev. Biophys. Biomol. Struct. 31 (2002) 303–319.

[14] M. Nitsch, J. Walz, D. Typke, M. Klumpp, L.-O. Essen, W. Baumeister, Group II chaperonin in an open conformation examined by electron tomography, Nat. Struct. Biol. 5 (1998) 855–857.

[15] J. Walz, T. Tamura, N. Tamura, R. Grimm, W. Baumeister, A.J. Koster, Tricorn protease exists as an icosahedral supermolecule in vivo, Mol. Cell 1 (1997) 59–65.

[16] A. Udvardy, Purification and characterization of a multiprotein component of the Drosophila-26-S (1500 kDa) proteolytic complex, J. Biol. Chem. 268 (1993) 9055–9062.

[17] K. Dierksen, D. Typke, R. Hegerl, W. Baumeister, Towards automatic electron tomography .2. Implementation of autofocus and low-dose procedures, Ultramicroscopy 49 (1993) 109–120.

[18] S. Nickell, F. Förster, A. Linaroudis, W. Del Net, F. Beck, R. Hegerl, W. Baumeister, J.M. Plitzko, TOM software toolbox: acquisition and analysis for electron tomography, J. Struct. Biol. 149 (2005) 227–234.

[19] A.M. Roseman, Particle finding in electron micrographs using a fast local correlation algorithm, Ultramicroscopy 94 (2003) 225–236.

[20] W.O. Saxton, W. Baumeister, The correlation averaging of a regularly arranged bacterial-cell envelope protein, J. Microsc.-Oxford 127 (1982) 127–138.

[21] P.A. Penczek, R.A. Grassucci, J. Frank, The ribosome at improved resolution—new techniques for merging and orientation refinement in 3d cryoelectron microscopy of biological particles, Ultramicroscopy 53 (1994) 251–270.

[22] J. Lowe, D. Stock, R. Jap, P. Zwickl, W. Baumeister, R. Huber, Crystal-structure of the 20S proteasome from the archaeon T-acidophilum at 3.4 Å resolution, Science 268 (1995) 533–539.

[23] D.M. Smith, G. Kafri, Y.F. Cheng, D. Ng, T. Walz, A.L. Goldberg, ATP binding to PAN or the 26S ATPases causes association with the 20S proteasome, gate opening, and translocation of unfolded proteins, Mol. Cell 20 (2005) 687–698.

[24] J. Ortega, H.S. Lee, M.R. Maurizi, A.C. Steven, ClpA and ClpX ATPases bind simultaneously to opposite ends of ClpP peptidase to form active hybrid complexes, J. Struct. Biol. 146 (2004) 217–226.

[25] M. Rohrwild, G. Pfeifer, U. Santarius, S.A. Muller, H.C. Huang, A. Engel, W. Baumeister, A.L. Goldberg, The ATP-dependent HsIVU protease from *Escherichia coli* is a four-ring structure resembling the proteasome, Nat. Struct. Biol. 4 (1997) 133–139.